Anomalous Optical Phonon Splittings in Sliding Bilayer Graphene

Seon-Myeong Choi,[†] Seung-Hoon Jhi,[‡,*] and Young-Woo Son[†,*]

[†]Korea Institute for Advanced Study, Seoul 130-722, Korea and [‡]Department of Physics and Division of Advanced Materials Science, Pohang University of Science and Technology, Pohang 790-784, Korea

ABSTRACT We study the variations of electron–phonon coupling and their spectroscopic consequences in response to the sliding of two layers in bilayer graphene using first-principles calculations and a model Hamiltonian. Our study shows that the long wavelength optical phonon modes change in a sensitive and unusual way depending on the symmetry as well as the parity of sliding atomic structures and that, accordingly, Raman- and infrared-active optical phonon modes behave differently upon the direction and size of the sliding. The renormalization of phonon modes by the interlayer electronic coupling is shown to be crucial to explain their anomalous behavior upon the sliding. Also, we show that the crystal symmetry change due to the sliding affects the polarized Stokes Raman scattering intensity, which can be utilized to detect tiny misalignment of graphene layers using spectroscopic tools.

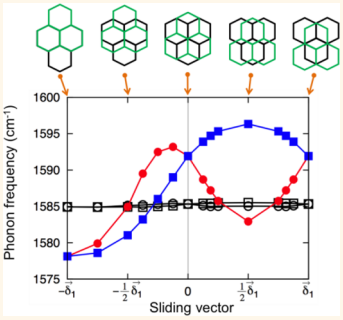

KEYWORDS: bilayer graphene · electron–phonon interaction · density functional theory

Successful isolation of graphene[1] and subsequent experiments that reveal its special properties[2,3] have generated excitement to explore the novel properties of the two-dimensional (2D) crystal from various disciplines. Advances in synthesis and experimental techniques enable the finding of other 2D crystals[4] and the artificial fabrication of multiply stacked structures.[5] Often, the stacking structures lead to very unusual electronic properties different from those of constituent 2D crystals depending on how they are piled up. Among them, bilayer graphene (BLG), which is a stacked structure of two single-layer graphene (SLG) sheets, is unique in electronic structure and exhibits colorful variation in low-energy states when its layer stacking is changed. The in-plane three-fold rotational and mirror symmetries and the decoupling of strong σ and weak π bondings of carbon atoms authorize the uniqueness of graphene systems. As such, the interlayer coupling in BLG, while a weak van der Waals type, produces interesting variations in low-energy band structures upon changes of stacking geometries. For example, its low-energy states in the Bernal-stacked pristine form[6] have quadratic energy bands but change to have linear bands when there is a rotational stacking fault.[7−9] Also, a sensitive electronic topological transition is also predicted for sliding systems.[10−12] Interplay of the interlayer interaction, the electron–phonon coupling, and the stacking fault by layer slidings are thus expected to produce drastic changes in its low-energy properties. Control of its electronic property is also enabled by manipulating such changes.

Recently, an epitaxially grown BLG on the vicinal surfaces of silicon carbide shows misalignment between two graphene layers exhibiting a complex nature of its electronic structures.[13] Moreover, recent experiments on CVD bi- and trilayer graphene also reveal possible misaligned layers at the domain walls between two ideally stacked graphene systems.[14,15] Immediate questions are how such structural variations are reflected in spectroscopic features and whether the misalignment of layers can be detected or not. Raman and infrared (IR) spectroscopies have proven to be powerful nondestructive methods to study physical and chemical properties of 2D crystals.[16−18] Physical properties of graphene under various conditions such as doping or mechanical strains have been verified using such tools.[16−20] In consideration of the rapid progress of research in this field,[10−15] comprehensive analysis of the spectroscopic features of sliding BLG will provide key information on the stacking geometry, the electron–phonon interactions, and low-energy excitations.

* Address correspondence to jhish@postech.ac.kr (S.-H.J.), hand@kias.re.kr (Y.-W.S.).

Received for review May 19, 2013 and accepted July 16, 2013.

Published online July 16, 2013
10.1021/nn402526r

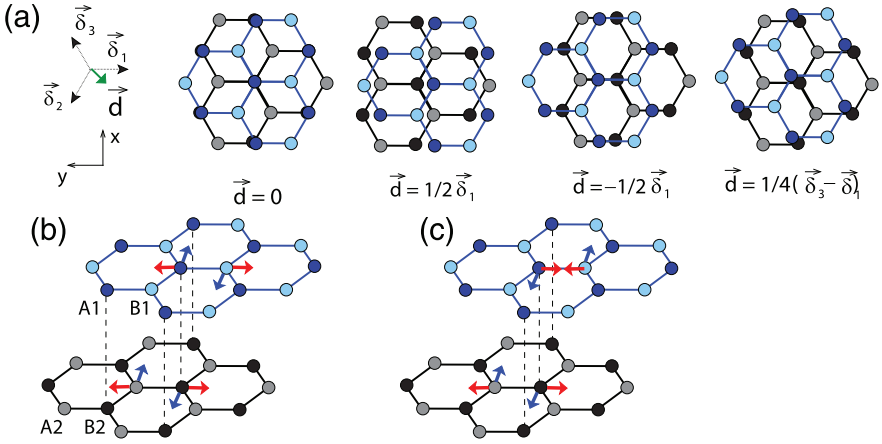

Figure 1. (a) Vectors $\vec{\delta}_i$ ($i = 1-3$) connecting the nearest-neighbor carbon atoms in each layer. The sliding vector in the upper layer is denoted by $\vec{d}$. From left to right, top views of BLG for $\vec{d}$ = 0, $1/2\vec{\delta}_1$, $-1/2\vec{\delta}_1$, and $1/4(\vec{\delta}_1 - \vec{\delta}_2)$. In-plane atomic displacements for (b) E_g and (c) E_u optical phonons, respectively. For each phonon mode, doubly degenerate atomic motions are denoted by red (LO mode) or blue (TO mode) arrows with carbon atoms of the same color moving in the same direction. Vertical dashed lines are guides for the eyes to the nearest interlayer carbon atoms (A2 and B1).

In this paper, we study long wavelength optical phonon modes responsible for Raman and IR spectra when two layers of BLG slide next to each other. We investigate how the tiny atomic misalignment between two layers changes its phonon frequencies and spectroscopic spectrum using first-principles calculations. It is found that the degeneracy of IR-active modes is immediately lifted by the sliding and each mode changes separately depending on sliding geometries. Unlike the behavior of IR modes, the frequencies of doubly degenerate Raman-active optical phonons do not change at all in all sliding circumstances. Such unconventional optical phonon splittings originate from the difference in their frequency renormalizations due to interlayer couplings, which is confirmed by our effective model Hamiltonian calculations. Moreover, we demonstrate that, owing to its changes in the crystal symmetry, nonresonant Stokes Raman scattering intensities associated with Raman-active phonons exhibit a strong polarization dependence so that they can be used to detect sub-angstrom misalignment between two layers in sliding BLG.

RESULTS AND DISCUSSION

Figure 1 illustrates the sliding geometry of graphene layers in BLG. When the sliding vector $\vec{d}$ is along $-\vec{\delta}_1$, the BLG gradually transforms from its pristine form of AB stacking (designated as AB-BLG) to AA stacking ($\vec{d} = -\vec{\delta}_1$) in which all carbon atoms are right on top of each other (AA-BLG). For the sliding along $+\vec{\delta}_1$, the AB-BLG becomes upside-down AB-stacked BLG (BA-BLG). Equivalent layer stackings are arranged by other sliding vectors along either $\pm\vec{\delta}_2$ or $\pm\vec{\delta}_3$ direction. Also, a combination of the sliding vectors is possible, as drawn in Figure 1a.

Among the phonon modes at the Γ-point in the Brillouin zone (BZ) of AB-BLG, high-frequency E_g (Figure 1b) and E_u optical modes (Figure 1c) are responsible for the Raman G-band and IR peak, respectively.[17,18] The in-plane atomic motions in the upper and lower layers (Figure 1b,c) are in-phase and out-of-phase for E_g and E_u modes, respectively. These modes are doubly degenerate as denoted by thick red arrows for longitudinal optical (LO) mode and by blue ones for transverse optical (TO) mode, as shown in Figure 1b,c. Our calculated phonon frequencies of E_u and E_g modes in AB-BLG are 1592 and 1585 cm^{-1}, respectively (Figure 2), in good agreement with previous studies.[21−23] As these two modes involve the interlayer interaction as well as the crystal symmetry, the sliding motion of two graphenes will imprint its effect on these modes.

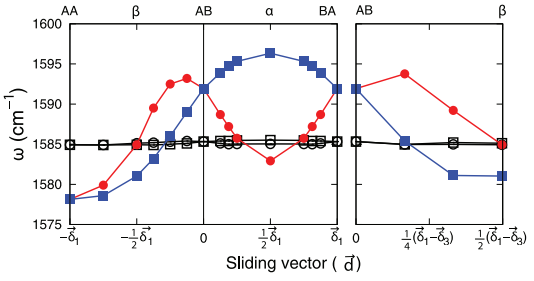

Figure 2. Variation of optical phonon frequencies as a function of sliding distance and direction. Red filled circles (blue filled rectangles) are frequencies for IR-active LO (TO) modes, and black empty circles and empty rectangles denote two Raman-active modes. The sliding vectors are shown in the bottom abscissa and corresponding stacking geometries in the top. The α-stacking ($\vec{d} = 1/2\vec{\delta}_1$) and β-stacking [$\vec{d} = -1/2\vec{\delta}_1$ or $1/2(\vec{\delta}_1 - \vec{\delta}_3)$] geometries are shown in the second and third panels of Figure 1a, respectively.

First, we find that the sliding in AB-BLG lifts the degeneracy of optical phonon modes immediately with the splitting size depending on both the sliding geometries and the symmetry of the phonon modes (Figure 2). The degeneracy is recovered when the

sliding ends up in AA-BLG (Figure 2). This finding is readily understood from the crystal symmetry of AB- and AA-BLG that guarantees the degeneracy of TO and LO modes for E_u and E_g phonons. However, E_g and E_u phonon modes exhibit completely different responses to the sliding because of their atomic motions (one in-phase and the other out-of-phase). The frequencies of IR-active E_u phonon modes are apparently split into two modes upon sliding, with a strong dependence on the sliding vectors (Figure 2). On the other hand, the frequencies of Raman-active E_g modes are seemingly unaffected at all by the sliding motion, although the exact degeneracy does not hold any more as Figure 2 illustrates. We observe that the splitting between TO and LO phonons is as large as 20 cm^{-1} for the E_u mode but no more than 1 cm^{-1} for the E_g mode.

To understand the intriguing behavior of optical phonons upon the sliding, we construct a minimal model of the phonon modes in sliding BLG. From our *ab initio* calculations for in-plane atomic displacements, we find that the interlayer ion−ion interaction energy changes very little (less than 10%) compared with the interlayer ion−electron interaction. So, additional force constants that account for the renormalization of in-plane phonon frequencies by the interlayer electronic hopping are sufficient to include into the conventional force constant model. Within the harmonic approximation, the phonon frequency of BLG ($\omega_\pm$ for $E_{g(u)}$ mode) at the Γ-point can be expressed as $\omega_\pm^2 = \omega_G^2 + \xi_\pm/m_c$, where ω_G is the frequency of E_{2g} phonon modes of SLG and $\xi_\pm$ is the effective force constant for the $E_{g(u)}$ phonon renormalization owing to the interlayer electron hoppings in BLG ($m_c \simeq 1.99 \times 10^{-23}$ g is the mass of the carbon atom).[24] The Hamiltonian for BLG with a sliding vector $\vec{d} = (d_x d_y)$[10−12] can be written as $H_{total} = H_{intra} + H_{inter}$, where the intralayer Hamiltonian is $H_{intra} = \Sigma_\alpha \Pi_{\vec{p}} c^\dagger_{B\alpha}(\vec{p}) c_{A\alpha}(\vec{p}) + (h.c.)$ and interlayer interaction $H_{inter} = \pi_{\vec{p}}(\vec{d}) c^\dagger_{B1}(\vec{p}) c_{A2}(\vec{p}) - \gamma_1 c^\dagger_{A1}(\vec{p}) c_{B2}(\vec{p}) + (h.c.)$. Here $c_{A\alpha}(c^\dagger_{B\alpha})$ is an annihilation (creation) operator for electron at site $A\alpha$ ($B\alpha$) in the upper and lower layers ($\alpha = 1,2$). $\Pi_{\vec{p}} = (3a_c t)/(2\hbar)(p_x + ip_y)$ and $\pi_{\vec{p}}(\vec{d}) = (3a_c\gamma_3)/(2\hbar)[p_x + ip_y - \beta(d_y - id_x)]$ where $t \simeq 3.0$ eV is the nearest-neighbor (nn) intralayer hopping constant, a_c the intralayer nn distance, $\gamma_1 (\simeq t/10)$ and $\gamma_3 (\simeq \gamma_1)$ the nn and the next nn interlayer hoppings, respectively, and $\beta \sim a_c^{-2}$.[10−12] With an intralayer electron−phonon coupling constant of $g \simeq 58$ eV/nm,[25,26] the Hamiltonian with the phonons can be described by changing $\Pi_{\vec{p}}$ to $\Pi_{\vec{p}}(u) = (3a_c t)/(2\hbar)(p_x + ip_y) + 3ug$ for the LO mode and to $\Pi_{\vec{p}}(u) = (3a_c t)/(2\hbar)(p_x + ip_y) - 3iug$ for the TO mode.[25,26] Here u is the amplitude of the E_{2g} phonon modes in SLG, and then the atomic displacements at A and B sites in the layer α are given as $\vec{u}_{A\alpha} = -\vec{u}_{B\alpha} = u\hat{y}$ (=$u\hat{x}$) for the LO (TO) mode (Figure 1b). With $\gamma_{1(3)}(u) \simeq \gamma_{1(3)} + \mathcal{O}(u^2)$, $\xi_\pm$ is obtained from the energy variation with respect to the atomic displacement

$$\xi_\pm = \frac{1}{2}\frac{g_v g_s}{S_c}\frac{\partial^2}{\partial u^2}\int_{S_c} d\vec{p}^{\,2}[E^\pm_{\vec{p}}(u) - E^S_{\vec{p}}(u)] \qquad (1)$$

where $E^\pm_{\vec{p}}(u) = -[|\Pi_{\vec{p}}(u)|^2 + |\Pi_{\vec{p}}(\pm u)|^2 + |\pi_{\vec{p}}(\vec{d})|^2 + \gamma_1^2 + 2|\Pi_{\vec{p}}(u)\Pi_{\vec{p}}(\pm u) + \gamma_1\pi^*_{\vec{p}}(\vec{d})|]^{1/2}$ and $E^S_{\vec{p}}(u) = -2|\Pi_{\vec{p}}(u)|$. $E^\pm_{\vec{p}}(u)$ corresponds to the energy of sliding BLG with E_g and E_u optical phonon modes, respectively, which can be obtained by direct diagonalization of H_{total}; $g_v = g_s = 2$ are the valley and spin degeneracy, respectively, and $S_c = \pi p_c^2 = (2^2\pi^2)/(3^{3/2}a_c^2)$ is half the BZ area accounting for the valley degeneracy.[24] In eq 1, the intralayer electron−phonon contribution $[E^S_{\vec{p}}(u)]$ of two graphene layers is subtracted from the energy of BLG with phonons $[E^\pm_{\vec{p}}(u)]$ to obtain the renormalized interlayer force constant only since ω_G is assumed to already be the renormalized intralayer phonon frequency.

The interlayer force constant ξ_+ becomes negligible for E_g phonon modes regardless of sliding (*i.e.*, $\omega_+ \simeq \omega_G$). This can be demonstrated easily by shifting $\vec{p}$ to $\vec{p} - (2\hbar ug/(a_c t),0)$ and $p + (0,2\hbar ug/(a_c t))$ for LO and TO E_g modes in eq 1, respectively. So, this explains the reason why sliding does not change the frequency of E_g modes. In contrast, for E_u modes of AB-BLG without sliding, we find $\xi_- \simeq (3\sqrt{3}g^2\gamma_1)/(\pi t^2)$ so that $\omega_-(\vec{d} = 0) - \omega_+ \simeq (1/2\omega_G)(3\sqrt{3}g^2\gamma_1)/(\pi m_c t^2) \sim 10$ cm^{-1} in a good agreement with our calculation in Figure 2. With sliding along $\vec{d} = \alpha\vec{\delta}_1$ ($|\alpha| \ll 1$), we find that $\Delta\omega_-(\vec{d}) \equiv \omega_-(\vec{d}) - \omega_-(\vec{d} = 0) \propto \mp(\Lambda/2\omega_G)(g^2\gamma_1\gamma_3)/(m_c t^3)\alpha$ for the LO (TO) E_u mode (here Λ is a dimensionless constant), which shows the splitting of two degenerate IR-active modes upon sliding, as shown in Figure 2. These calculations explain the different responses of Raman-active and IR-active phonon modes in sliding BLG.

Having understood the origin of the anomalous optical phonon splittings upon sliding, we investigate their spectroscopic consequences. Our calculations readily indicate that the sliding systems have different IR reflectivity and Raman spectrum when it is placed on insulating substrates with top or bottom gates. The single Fano-like IR spectra of gated BLG[18] will turn into the double-peak spectrum upon sliding because of the splitting in E_u phonon frequencies. Also, its anomalous splitting in the Raman G-band[25−28] due to mixing between E_g and E_u modes will be affected by sliding. The splitting of the Raman G-band (or spectral transfer between opposite parity optical phonon modes) of gated BLG is known to originate from the inversion symmetry breaking by the gate electric field.[25,26] Therefore, we expect that the splitting in the E_u mode upon sliding will generate a more complex Raman spectrum in the gated structure (*e.g.*, a three-peak structure). While the gated structure is the most straightforward way to observe the sliding-induced

TABLE 1. Calculated Raman Tensors for Various Sliding Vectors ($\vec{d}$)[a]

$\vec{d}$	G	Raman tensors, R_ν (ν = 1,2)	
0	D_{3d}	$E_g\begin{pmatrix} c & 0 \\ 0 & -c \end{pmatrix} E_g\begin{pmatrix} 0 & d \\ d & 0 \end{pmatrix}$	$c = -d = 1.00$
$-\vec{\delta}_1$	D_{6h}	$E_{2g}\begin{pmatrix} c & 0 \\ 0 & -c \end{pmatrix} E_{2g}\begin{pmatrix} 0 & d \\ d & 0 \end{pmatrix}$	$c = d = 1.11$
$1/2\vec{\delta}_1$	D_{2h}	$A_g\begin{pmatrix} a & 0 \\ 0 & b \end{pmatrix} B_{1g}\begin{pmatrix} 0 & d \\ d & 0 \end{pmatrix}$	$a = +1.07, b = -0.88, d = -0.97$
$-3/4\vec{\delta}_1$	C_{2h}	$A_g\begin{pmatrix} a & 0 \\ 0 & b \end{pmatrix} A_g\begin{pmatrix} 0 & d \\ d & 0 \end{pmatrix}$	$a = +1.09, b = -1.13, d = -1.11$
$-1/2\vec{\delta}_1$			$a = +0.95, b = -0.98, d = -1.07$
$-1/4\vec{\delta}_1$			$a = +0.91, b = -0.90, d = -1.00$
$+1/4\vec{\delta}_1$			$a = +0.95, b = -0.91, d = -0.96$
$+1/3\vec{\delta}_M$			$a = +0.99, b = -0.92, d = -1.01$
$+1/6\vec{\delta}_M$	C_i	$A_g\begin{pmatrix} a & c \\ c & b \end{pmatrix} A_g\begin{pmatrix} a' & c' \\ c' & b' \end{pmatrix}$	$a = -0.91, b = +0.88, c = -0.39, a' = -0.33, b' = +0.32, c' = +0.87$

[a] G is the Schoenflies notation of the point-group symmetry for each sliding geometry. Here, $\vec{\delta}_M = \vec{\delta}_1 - \vec{\delta}_3$. The components of all Raman tensors expressed in the vibrational symmetry group notations are normalized to the AB-BLG Raman tensor.

splitting of optical phonons, more generic ways are desirable of detecting tiny sliding on arbitrary substrates without the need for heavy doping using the field-effect transistor structure. We present below that conventional Raman techniques with polarizers can indeed detect sub-angstrom atomic misalignment by sliding.

The position of the Raman G-band of sliding BLG does not change at all for all sliding configurations, but the change in the crystal symmetry produces very interesting movement of the Raman intensity. In order to calculate the nonresonant Stokes Raman intensity of the G-band, we used the Placzek approximation for the Raman intensity (I) as $I \propto d\sigma/d\Omega = \Sigma_{\nu=1,2}|\mathbf{e}_i \cdot \mathbf{R}_\nu \cdot \mathbf{e}_s|^2$.[29−31] Here $\mathbf{R}_\nu$ is the Raman tensor, $\mathbf{e}_i$ and $\mathbf{e}_s$ are the polarization of the incident and scattered lights, respectively.[29−31] $\mathbf{R}_\nu$ associated with the doubly degenerate Raman-active phonon modes is proportional to the Raman susceptibility α^ν_{ij}, which is defined as $\alpha^\nu_{ij} = \Sigma_{lk}(\partial\chi_{ij})/(\partial r_{lk})u^\nu_{lk}$. Here, u^ν_{lk} is the νth phonon eigenvector of the lth atom along the k direction, and χ_{ij} is the electric polarizability tensor ($i,j,k = x,y$, as we neglect the irrelevant z component).[29−31] We directly calculate the derivative of χ_{ij} with respect to the atomic displacements corresponding to the νth modes. Assuming an incident light with an energy of 2.41 eV, calculated Raman tensors for various sliding geometries are summarized in Table 1 together with corresponding crystal symmetry groups and vibrational symmetries.[32] Our calculations of Raman tensors for AB-BLG and AA-BLG reproduce the well-known results with E_g and E_{2g} symmetries.[32,33] Upon sliding, changes in the crystal symmetry produce correspondingly distinctive Raman

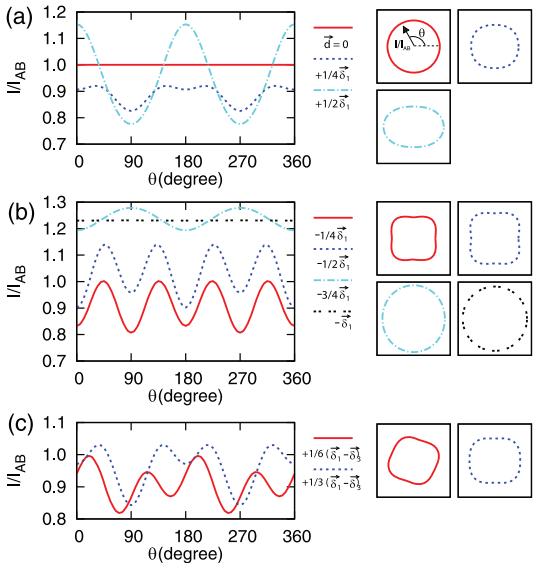

Figure 3. Polarization dependence of the Raman G-band intensity in BLG with a sliding along (a) $+\vec{\delta}_1$, (b) $-\vec{\delta}_1$, and (c) $+(\vec{\delta}_1 - \vec{\delta}_3)$ directions. The panels in the left show the Raman intensity normalized to that of AB-BLG as a function of polarization angle (θ), and small rectangular panels on the right show corresponding polar plots.

tensors. With $\mathbf{e}_i = \mathbf{e}_s = (\cos\theta, \sin\theta)$, the polarized Raman intensity for AB-BLG is given as $I = |c(\cos^2\theta - \sin^2\theta)|^2 + |2c\sin\theta\cos\theta|^2 \equiv I_{AB}$ so that the intensity does not depend on the polarization angle θ (Figure 3a).[32,33] This behavior is also the same for AA-BLG while with a different intensity. When the sliding direction ($\vec{d}$) is along $\pm\delta_1$, the polarized Raman intensity is given as $I(\theta)/I_{AB} = ((a-b)^2)/(8)\cos 4\theta + (a^2 - b^2 - d^2)/(2)\cos 2\theta + I_0$ (a,b, and d are given in Table 1, and I_0 is a

constant). $I(\theta)$ has an elliptic shape for $a \approx b$ or quadrupolar form otherwise, as shown in Figure 3. When $\vec{d}$ deviates from the direction of $\pm\delta_1$, the polarized intensity tends to rotate, as shown in Figure 3c. In case the overall shape of the polarized intensity looks similar, its magnitude has a strong dependence on the sliding size (Figure 3b).

CONCLUSIONS

In conclusion, we have shown theoretically that tiny sliding of the layers in BLGs can induce anomalous splitting of the optical phonon that changes the spectroscopic features significantly. We have shown that the frequencies of the degenerate in-phase optical phonons (E_g mode) are hardly changed irrespective of sliding distance and direction. On the other hand, the polarization-dependent Raman intensity associated with the E_g mode is modified strongly so that the sub-angstrom misalignment between two graphene layers can be resolved by spectroscopic methods. We expect that this study will provide essential information for spectroscopic measurements and for linking local atomic structures to novel electronic properties of stacked 2D atomic crystals.

THEORETICAL METHODS

We calculated electronic structures and phonon dispersions of the sliding BLGs using first-principles methods with a plane-wave basis set.[34] The local density approximation is adopted for the exchange-correlation functional, and the phonon frequencies are calculated using the density functional perturbation theory.[35] Computations are also repeated using the atomic orbital basis set,[36] the generalized gradient approximation (GGA),[37] and frozen phonon method[36] to find almost identical results. In calculating electronic structures and phonon dispersions with the atomic orbital basis set, the basis set superposition errors were removed by including two ghost atoms in the unit cell.[38] A semiempirical correction of van der Waals (vdW) forces is added to all our calculations following Grimme's proposal, which is essential to obtain the correct interlayer distance of sliding BLGs.[10,39] We note that our methods accurately describe the phonon frequencies of graphitic systems when the appropriate interlayer distance is provided.[21,22]

Conflict of Interest: The authors declare no competing financial interest.

Acknowledgment. S.-M.C. thanks C.-H. Park for discussions. Y.-W.S. is supported by the NRF of Korea grant funded by MEST (QMMRC, No. R11-2008-053-01002-0 and Nano R&D program 2008-03670). S.-H.J. acknowledges the support from the NRF of Korea grant funded by MEST (SRC Program No. 2011-0030046 and WCU program No. R31-2008-000-10059). Computational resources have been provided by KISTI Supercomputing Center (Project No. KSC-2011-C1-21) and the CAC of KIAS.

REFERENCES AND NOTES

1. Novoselov, K. S.; Geim, A. K.; Morozov, S. V.; Jiang, D.; Zhang, Y.; Dubonos, S. V.; Grigorieva, I. V.; Firsov, A. A. Electric Field Effect in Atomically Thin Carbon Films. *Science* **2004**, *306*, 666–669.
2. Novoselov, K. S.; Geim, A. K.; Morozov, S. V.; Jiang, D.; Katsnelson, M. I.; Grigorieva, I. V.; Dubonos, S.; Firsov, A. A. Two-Dimensional Gas of Massless Dirac Fermions in Graphene. *Nature* **2005**, *438*, 197–200.
3. Zhang, Y.; Tan, Y.-W.; Stormer, H. L.; Kim, P. Experimental Observation of the Quantum Hall Effect and Berry's Phase in Graphene. *Nature* **2005**, *438*, 201–204.
4. Novoselov, K. S.; Jiang, D.; Schedin, F.; Booth, T. J.; Khotkevich, V. V.; Morozov, S. V.; Geim, A. K. Two-Dimensional Atomic Crystals. *Proc. Natl. Acad. Sci. U.S.A.* **2005**, *102*, 10451–10453.
5. Novoselov, K. S. Nobel Lecture: Graphene: Materials in the Flatland. *Rev. Mod. Phys.* **2011**, *83*, 837–849.
6. McCann, E.; Fal'ko, V. I. Landau-Level Degeneracy and Quantum Hall Effect in a Graphite Bilayer. *Phys. Rev. Lett.* **2006**, *96*, 086805.
7. Lopes dos Santos, J. M. B.; Peres, N. M. R.; Castro Neto, A. H. Graphene Bilayer with a Twist: Electronic Structure. *Phys. Rev. Lett.* **2007**, *99*, 256802.
8. Hass, J.; Varchon, F.; Millán-Otoya, J. E.; Sprinkle, M.; Sharma, N.; de Heer, W. A.; Berger, C.; First, P. N.; Magaud, L.; Conrad, E. H. Why Multilayer Graphene on 4*H*−SiC-(000$\bar{1}$) Behaves Like a Single Sheet of Graphene. *Phys. Rev. Lett.* **2008**, *100*, 125504.
9. Shallcross, S.; Sharma, S.; Pankratov, O. A. Quantum Interference at the Twist Boundary in Graphene. *Phys. Rev. Lett.* **2008**, *101*, 056803.
10. Son, Y.-W.; Choi, S.-M.; Hong, Y. P.; Woo, S.; Jhi, S.-H. Electronic Topological Transition in Sliding Bilayer Graphene. *Phys. Rev. B* **2011**, *84*, 155410.
11. Mucha-Kruczyński, M.; Aleiner, I. L.; Fal'ko, V. I. Strained Bilayer Graphene: Band Structure Topology and Landau Level Spectrum. *Phys. Rev. B* **2011**, *84*, 041404.
12. de Gail, R.; Goerbig, M. O.; Montambaux, G. Magnetic Spectrum of Trigonally Warped Bilayer Graphene: Semiclassical Analysis, Zero Modes, and Topological Winding Numbers. *Phys. Rev. B* **2012**, *86*, 045407.
13. Hicks, J.; Tejeda, A.; Taleb-Ibrahimi, A.; Nevius, M. S.; Wang, F.; Shepperd, K.; Palmer, J.; Bertran, F.; Le Fevre, P.; Kunc, J.; *et al.* A Wide-Bandgap Metal-Semiconductor- Metal Nanostructure Made Entirely from Graphene. *Nat. Phys.* **2013**, *9*, 49–54.
14. Brown, L.; Hovden, R.; Huang, P.; Wojcik, M.; Muller, D. A.; Park, J. Twinning and Twisting of Tri- and Bilayer Graphene. *Nano Lett.* **2012**, *12*, 1609–1615.
15. Hattendorf, S.; Georgi, A.; Liebmann, M.; Morgenstern, M. Network of ABA and ABC Stacked Graphene on Mica Observed by Scanning Tunneling Microscopy. *Surf. Sci.* **2013**, *610*, 53–58.
16. Saito, R.; Hofmann, M.; Dresselhaus, G.; Jorio, A.; Dresselhaus, M. S. Raman Spectroscopy of Graphene and Carbon Nanotubes. *Adv. Phys.* **2011**, *60*, 413.
17. Ferrari, A. C.; Meyer, J. C.; Scardaci, V.; Casiraghi, C.; Lazzeri, M.; Mauri, F.; Piscanec, S.; Jiang, D.; Novoselov, K. S.; Roth, S.; *et al.* Raman Spectrum of Graphene and Graphene Layers. *Phys. Rev. Lett.* **2006**, *97*, 187401.
18. Kuzmenko, A. B.; Benfatto, L.; Cappelluti, E.; Crassee, I.; van der Marel, D.; Blake, P.; Novoselov, K. S.; Geim, A. K. Gate Tunable Infrared Phonon Anomalies in Bilayer Graphene. *Phys. Rev. Lett.* **2009**, *103*, 116804.
19. Mohiuddin, T. M. G.; Lombardo, A.; Nair, R. R.; Bonetti, A.; Savini, G.; Jalil, R.; Bonini, N.; Basko, D. M.; Galiotis, C.; Marzari, N.; *et al.* Uniaxial Strain in Graphene by Raman Spectroscopy: *G* Peak Splitting, Grüneisen Parameters, and Sample Orientation. *Phys. Rev. B* **2009**, *79*, 205433.
20. Yoon, D.; Son, Y.-W.; Cheong, H. Strain-Dependent Splitting of the Double-Resonance Raman Scattering Band in Graphene. *Phys. Rev. Lett.* **2011**, *106*, 155502.
21. Mounet, N.; Marzari, N. First-Principles Determination of the Structural, Vibrational and Thermodynamic Properties of Diamond, Graphite, and Derivatives. *Phys. Rev. B* **2005**, *71*, 205214.
22. Tan, P. H.; Han, W. P.; Zhao, W. J.; Wu, Z. H.; Chang, K.; Wang, H.; Wang, Y. F.; Bonini, N.; Marzari, N.; Pugno, N.; *et al.*

The Shear Mode of Multilayer Graphene. *Nat. Mater.* **2012**, *11*, 294.
23. Yan, J.-A.; Ruan, W. Y.; Chou, M. Y. Phonon Dispersions and Vibrational Properties of Monolayer, Bilayer, and Trilayer Graphene: Density-Functional Perturbation Theory. *Phys. Rev. B* **2008**, *77*, 125401.
24. Samsonidze, G. G.; Barros, E. B.; Saito, R.; Jiang, J.; Dresselhaus, G.; Dresselhaus, M. S. Electron−Phonon Coupling Mechanism in Two-Dimensional Graphite and Single-Wall Carbon Nanotubes. *Phys. Rev. B* **2007**, *75*, 155420.
25. Ando, T. Anomaly of Optical Phonons in Bilayer Graphene. *J. Phys. Soc. Jpn.* **2007**, *76*, 104711.
26. Ando, T.; Koshino, M. Field Effects on Optical Phonons in Bilayer Graphene. *J. Phys. Soc. Jpn.* **2009**, *78*, 034709.
27. Malard, L. M.; Elias, D. C.; Alves, E. S.; Pimenta, M. A. Observation of Distinct Electron−Phonon Couplings in Gated Bilayer Graphene. *Phys. Rev. Lett.* **2008**, *101*, 257401.
28. Yan, J.; Villarson, T.; Henriksen, E. A.; Kim, P.; Pinczuk, A. Optical Phonon Mixing in Bilayer Graphene with a Broken Inversion Symmetry. *Phys. Rev. B* **2009**, *80*, 241417.
29. Brüesch, P. *Phonons: Theory and Experiments II*; Springer: Berlin, 1986.
30. Porezag, D.; Pederson, M. R. Infrared Intensities and Raman-Scattering Activities within Density-Functional Theory. *Phys. Rev. B* **1996**, *54*, 7830–7836.
31. Umari, P.; Pasquarello, A. Infrared and Raman Spectra of Disordered Materials from First-Principles. *Diamond Relat. Mater.* **2005**, *14*, 1255.
32. Loudon, R. The Raman Effect in Crystals. *Adv. Phys.* **1964**, *13*, 423.
33. Yoon, D.; Moon, H.; Son, Y.-W.; Samsonidze, G.; Park, B. H.; Kim, J. B.; Lee, Y.; Cheong, H. Strong Polarization Dependence of Double-Resonant Raman Intensities in Graphene. *Nano Lett.* **2008**, *8*, 4270–4274.
34. Giannozzi, P.; Baroni, S.; Bonini, N.; Calandra, M.; Car, R.; Cavazzoni, C.; Ceresoli, D.; Chiarotti, G. L.; Cococcioni, M.; Dabo, I.; *et al.* QUANTUM ESPRESSO: A Modular and Open-Source Software Project for Quantum Simulations of Materials. *J. Phys.: Condens. Matter* **2009**, *21*, 395502.
35. Baroni, S.; de Gironcoli, S.; Dal Corso, A.; Giannozzi, P. Phonons and Related Crystal Properties from Density-Functional Perturbation Theory. *Rev. Mod. Phys.* **2001**, *73*, 515.
36. Soler, J. M.; Artacho, E.; Gale, J. D.; García, A.; Junquera, J.; Ordejón, P.; Sánchez-Portal, D. The SIESTA Method for *Ab Initio* Order-N Materials Simulation. *J. Phys.: Condens. Matter* **2002**, *14*, 2745.
37. Perdew, J. P.; Burke, K.; Ernzerhof, M. Generalized Gradient Approximation Made Simple. *Phys. Rev. Lett.* **1996**, *77*, 3865–3868.
38. Balabin, R. M. Enthalpy Difference between Conformations of Normal Alkanes: Intramolecular Basis Set Superposition Error (BSSE) in the Case of *n*-Butane and *n*-Hexane. *J. Chem. Phys.* **2008**, *129*, 164101.
39. Grimme, S. Semiempirical GGA-Type Density Functional Constructed with a Long-Range Dispersion Correction. *J. Comput. Chem.* **2006**, *27*, 1787.